11-10-2018

Axial Compressive Behavior of Square Ice Filled Steel Tubular Stub Columns

Yanlei Wang
Dalian University of Technology

Guipeng Chen
Dalian University of Technology

Baolin Wan
Marquette University, baolin.wan@marquette.edu

Hao Lin
Dalian University of Technology

Axial Compressive Behavior of Square Ice Filled Steel Tubular Stub Columns

Yanlei Wang

State Key Laboratory of Coastal and Offshore Engineering, School of Civil Engineering, Dalian University of Technology, Dalian 116024, China

Guipeng Chen

State Key Laboratory of Coastal and Offshore Engineering, School of Civil Engineering, Dalian University of Technology, Dalian 116024, China

Baolin Wan

Department of Civil, Construction and Environmental Engineering, Marquette University, Milwaukee, WI

Hao Lin

State Key Laboratory of Coastal and Offshore Engineering, School of Civil Engineering, Dalian University of Technology, Dalian 116024, China

Highlights

- Square IFT column is proposed to combine the advantages of ice and steel tube.
- Influence of width-to-thickness ratio of steel tubes on square IFT is analyzed.
- Bearing capacity of IFT increases with the decrease of width-to-thickness ratio.
- Good composite action between outer steel tube and ice core is achieved.
- Equations for predicting bearing capacity of square IFT columns are proposed.

Abstract

Concrete has many limitations in the building construction in cold areas. However, there is abundant ice in those regions. Therefore, using ice as a substitute for concrete has been explored by researchers. Inspired by the idea of square concrete filled steel tube (CFT), a new column form termed square ice filled steel tubular (IFT) column is proposed in this study. It consists of a square outer steel tube with the inner space filled with ice. A total of eighteen stub columns were made and tested under axial compression, including three circular plain ice specimens, nine square IFT specimens and six hollow square steel tubes, to demonstrate the advantages of the composite column. The width-to-thickness (B/t) ratio of the steel tubes varies from 39.5 to 77. The test results confirmed that the ice core is effectively confined by the steel tube, and the inward local buckling of the steel tube is suppressed by the inner ice, leading to higher strength and better ductility of the square IFT specimens compared with hollow steel tubes and plain ice columns. A simplified axial bearing capacity equation for square IFT stub columns is proposed and it provides reasonable and accurate predictions of the test results.

Keywords

Ice, Steel tube, Ice filled steel tube, Axial compression, Stub column

1. Introduction

It is difficult to mix, pour and cure concrete in cold regions such as Arctic areas, where the temperature is below 0 °C throughout the year. It is also very expensive to transport component materials of concrete to such areas. The idea of using ice as building materials was successfully achieved by Inuit people living near the North Pole [1]. The ongoing freezing and refreezing processes harden their igloos made of ice blocks, which confirms that the utilization of ice as a substitute for traditional building material (i.e., concrete) is feasible.

In the 1990's, many researches [2], [3], [4], [5], [6], [7], [8] were performed to study the compressive strength of ice. The impetus behind the research on ice was the development of the oil and gas industry in Arctic areas, the construction of hydropower infrastructures, and the design of icebreaker and lighthouse. Ice load is usually the predominant design criterion for hydro-structures used in cold regions, and the compressive strength of ice is a key parameter in the calculation of ice load [9]. In recent years, the research on the compressive behavior of ice is still ongoing. Ice is a material which is strong in compression and weak in tension, especially at colder temperatures well below the freezing point [10]. The mechanical properties of ice and snow were reviewed by Petrovic [11]. The tensile strength of ice was 0.7–3.1 MPa and the compressive strength was 5–25 MPa over the temperature range from −10 °C to −20 °C. The ice compressive strength increased with decreasing temperature and increasing strain rate, but the tensile strength was relatively insensitive to these variables. Ice strength depends on many variables such as temperature, strain rate, test specimen volume, and ice grain size [11]. Barrette and Jordaan [12] investigated the compressive behavior of freshwater ice (i.e., laboratory-grown ice and iceberg ice) subjected to a nominally constant compressive stress of 15 MPa while under confining pressures ranging from 10 to 65 MPa. Test temperature varied from about −5 to −26 °C. The iceberg

ice tended to show a higher scatter than the laboratory ice. Their results were consistent with those of other investigators [13], [14], [15], [16] obtained from constant strain rate experiments. The peak stresses of ice reported in the work by Dutta et al. [17] were 6.53 ± 1.44 MPa and 6.77 ± 3.23 MPa at −10 °C under quasi-static and dynamic loading conditions, respectively. Tests of uniaxial compression strength of columnar sea ice were conducted by Moslet [18] in field in Svalbard, Norway. Both horizontal and vertical samples were tested and the relationship between the strength and sample directions seemed not to be constant. However, the strength of sea ice was dependent on temperature [18]. Shazly et al. [19] studied the dynamic response of ice under uniaxial compression in the range of strain rates from 60 to 1400 s^{-1} and at initial test temperatures of −10 and −30 °C. According to the test results, the compressive strength of ice showed positive strain rate sensitivity over the employed range of strain rates. Moreover, unlike in the case of uniaxial quasi-static compression of ice, the effect of specimen end-constraint during the high rate compression was found to be negligible. Zhang et al. [9] investigated the strength of artificial freshwater ice under uniaxial compression with test parameters including temperature and strain rate. The results showed that the compressive strength of ice was very sensitive to the strain rate. The uniaxial compressive strength of ice increased with the decrease of experimental temperature at the same strain rate. More than 340 experiments were conducted by Zhang et al. [20] to study the compressive strength of reservoir ice at different temperatures and strain rates. The relationship among the uniaxial compressive strength of ice, strain rate and temperature was established. All aforementioned researches indicated that ice is a weak material and its mechanical properties are strongly dependent on temperature and strain rate. Therefore, plain ice is not a reliable material used for structural members subjected to large or explosive loads. Owing to its brittleness it was dangerous to regard any reasonable stresses as safe for constructional purposes [21].

In order to improve the behavior of plain ice, many methods have been tried to reinforce it. The Inuit people have traditionally reinforced the snow blocks for their igloos with lichen, and many ice roads across the northern Baltic built in the period of Soviet Union used sawdust as a reinforcing agent [22]. Nixon and Smith [22] tested a number of ice composites reinforced by some wood-based materials (i.e., newspaper, wood pulp, sawdust, blotting paper and crushed bark) to determine the fracture toughness of such composites. The test results showed that the fracture toughness of freshwater ice increased by 5–20 times after introducing 5–20% reinforcing materials in weight, and it was concluded that reinforced ice could be used as a construction material in Arctic regions [22]. Considering that it is expensive to transport reinforcing materials to Arctic areas, Nixon [23] suggested using alluvium as an alternative reinforcing agent, which is readily available either in the form of seabed silt in the Arctic offshore or from various onshore deposits. Test results showed that ice could be significantly strengthened by the addition of alluvium. The degree of strengthening was found to be dependent on both type and amount of the alluvium used. The bending strength of reinforced ice tended to increase with the decreasing particle size, and there existed one critical percentage of reinforcement, above which value considerably higher bending strength was obtained [23]. Vasiliev [24] studied the strength of ice strengthened by fiberglass net and fiberglass cloth. Specimens of reinforced and plain ice cubes with the dimension of 70 × 70 × 70 mm^3 were tested under uniaxial compression while the reinforced and plain ice beams with the dimension of 40 × 40 × 160 mm^3 were subjected to three-point bending. It was found that crack propagation in the reinforced ice was prevented by the reinforcing agents. Both the compressive and flexural strengths of ice were effectively increased after introducing fiberglass into ice. Nowadays there is a growing interest in the ice-soil composites created by the method of cryotropic gel formation (CGF) [25], [26], [27]. In the CGF method, strong hydrogels are formed from an aqueous polymer solution such as PVA; and other hydrogels are formed by means of a freezing and thawing process in which PVA solutions are frozen at −5 to −20 °C and then allowed to thaw at a positive temperature. Materials created by CGF method have low permeability, which has been used as a reliable material for building weirs and other hydraulic engineering constructions in cold regions [25]. According to the test results of Vasiliev et al. [26], the strength of the ice-soil composites depends on many

different factors, including the quality and quantity of PVA used, time of thawing, number of freezing-thawing cycles, soil characteristics, and water content of the soils with gel. Pykrete is another popular form of reinforced ice composites, which is a mixture of sawdust or some other form of wood pulp (such as paper) and ice. In view of the similarity to concrete and in honor of Mr. Geoffrey Pyke who firstly proposed the construction of aircraft carriers using ice, the mixture was given the code name of pykrete (Pyke's concrete) [21]. A total of 50 cylinders and 50 beams made of pykrete were manufactured and tested by Vasiliev et al. [28] to investigate both the compressive and flexural strengths of such composites. The compressive and flexural strengths of pykrete with 10% sawdust were 12 MPa and 3.7 MPa, respectively, which were three times as large as those of plain ice.

As shown in the previous discussion, the mechanical properties of plain ice can be improved with the introduction of some reinforcing materials into ice. However, the extent of improvement in the compressive strength of ice by this means is limited. The strength of reinforced ice is still lower than that of normal concrete and can not be used for structural members subjected to larger loads. Therefore, it is necessary to find alternative ways to help ice to achieve higher strength and better ductility. Recently, concrete filled steel tubular (CFT) members have been widely used in routine structural design as piles, building columns and bridge piers [29]. These columns have demonstrated excellent earthquake-resistant properties, namely high stiffness, high strength, high ductility, and large energy-absorption capacity [30]. The enhancement of structural properties of CFT columns is mainly due to the composite action of steel hollow section and concrete core. The confining effect from the steel hollow section causes the concrete core to behave in a triaxial stress state while the concrete core prevents the wall of the steel hollow section from buckling inward [31]. It should be noted that the circular cross-section provides the strongest confinement to the concrete core, and the local buckling is more likely to occur in square or rectangular cross-sections [32]. However, square and rectangular CFT columns are still increasingly used in civil engineering due to easier construction in beam-to-column connection, high cross-sectional bending stiffness and aesthetic reasons [32]. A lot of researches have been carried out on the behavior of square CFT columns under axial compression [33], [34], [35], [36] or bending load [37], [38], [39], [40]. Inspired by the idea of circular CFT columns, the authors innovatively proposed a new type of structural member termed circular ice filled steel tubular (IFT) column in which the concrete was replaced by ice [41]. The test results demonstrated that the circular steel tube worked well with the inner ice, leading to higher strength and better ductility of circular IFT columns than those of hollow steel tubes and plain ice columns.

Based on the existing studies on circular IFT columns [41] and square CFT columns [29], [32], an exploratory experimental study was designed to investigate the behavior of square IFT stub columns under axial compression. This study aimed to check whether the outer square steel tube could work well with the inner ice and to identify whether there is notable composite action between the two parts. An equation for predicting the ultimate bearing capacity of square IFT stub columns is also proposed in this paper.

2. Experimental program

2.1. Specimens

A total of eighteen specimens, including three circular plain ice columns, nine square IFT columns and six hollow square steel tubes, were prepared and tested under uniaxial compression. The main parameter investigated in this study was the width-to-thickness (B/t) ratio which varied from 39.5 to 77. The diameter and height of the three circular plain ice specimens were 150 mm and 300 mm, respectively. This size is similar to that of standardized cylindrical concrete specimens (diameter of 6 in. and height of 12 in.) for compression test. It should be noted that there is no code for designing ice structures and the results of nominally similar tests might vary greatly because different research groups use different samples and testing methods. In the ice engineering field, the Working Group of the IAHR Section on Ice Problems proposed its recommendations for standardized

testing methods to measure the mechanical properties of ice in 1981 [42]. The initial purpose of this guideline was not to use ice as a building material and some of its details do not meet the current requirements. It is difficult to control the strain rate by using the recommended method to test ice under uniaxial compression. However, the compressive strength of ice is very sensitive to the strain rate as discussed previously. Therefore, this guide was not used directly in this study. The three plain ice specimens were labeled as C01, C02 and C03, respectively. The letter C represented circular plain ice columns.

The nine square IFT specimens were divided into three series (i.e., b, c and d) and each series consisted of three identical IFT columns with the same thickness of steel tubes. The thicknesses of steel tube in series b, c and d were 2 mm, 3 mm and 4 mm, respectively. The square steel tube used in each square IFT specimen had the same inner side width of 150 mm, measured at the outer surface of the ice core, and a height of 300 mm. Therefore, all the square IFT specimens were stub columns with little influence from end effect and overall buckling. Each IFT specimen was given a name, which started with letter S standing for square IFT columns, followed by a number representing the thickness of steel tubes in mm, and the specimen number within the same series.

For each type of hollow steel tubes, two identical hollow steel tubes, which had the same dimensions as those in the corresponding square IFT specimens, were made and tested under uniaxial compression. According to a naming rule, each hollow steel tube was given a name. For example, in specimen H32, the letter H stood for hollow steel tubes, followed by a number of 3 representing that the thickness of the steel tube was 3 mm, and the last digit depicted that it was the second specimen tested among the two identical steel tubes. Details of all specimens are reported in Table 1.

Table 1. Details of specimens and test results.

Series	Specimen	B	t	B/t	E_s	f_y	f_u	N_e	N_u	N_u/N_e
		mm	mm		GPa	MPa	MPa	kN	kN	
a	C01	–	–	–	–	–	–	60.7	–	–
	C02	–	–	–	–	–	–	60.6	–	–
	C03	–	–	–	–	–	–	61.8	–	–
b	S21	154	2	77	206	274	402	412.1	408.5	0.99
	S22							412.6	408.5	0.99
	S23							404.9	408.5	1.01
	H21							330.1	–	–
	H22							328.0	–	–
c	S31	156	3	52	207	251	380	563.0	570.6	1.01
	S32							560.3	570.6	1.02
	S33							565.9	570.6	1.01
	H31							462.4	–	–
	H32							465.7	–	–
d	S41	158	4	39.5	209	230	351	724.3	709.3	0.98
	S42							706.4	709.3	1.00
	S43							720.9	709.3	0.98
	H41							590.2	–	–
	H42							581.7	–	–

Note: In this table, B is the width of square steel tube, t is the thickness of steel tube, N_e is the experimental results, and N_u is the calculated results.

2.2. Preparation of specimens

Each square steel tube was manufactured from two mild steel plates with the same thickness. The two plates were firstly rolled up into U shape, and then welded together. The corner radius of all square steel tubes was 8 mm. In addition, a 200 mm by 200 mm square steel end-plate with 10 mm thickness was welded to the bottom of each square steel tube (Fig. 1a). Waterproofness was checked by pouring some water into the finished tubes. For the hollow square steel tube specimens without inner ice, both ends were welded to a steel end-plate.

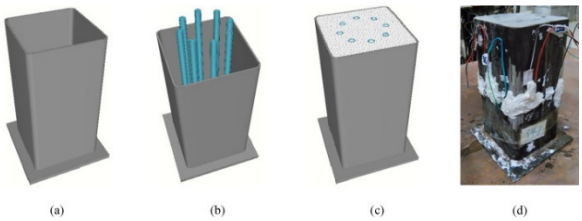

Fig. 1. Preparation of square IFT specimens: (a) steel formwork; (b) placement of PVC hoses; (c) schematic of IFT specimen; and (d) IFT specimen.

In contrast to traditional building materials such as normal concrete, ice has a unique feature that its volume expands by about 11% during the phase of water freezing. This natural law was ignored in our initial tests, leading to many cracks found in the trial specimens. It can be explained by the fact that the volume expansion of the ice core is firmly confined by the outer square steel tube and thus the expansive pressure can not be released. This problem was solved by trial and error. Eight flexible hollow PVC hoses with an inner diameter of 8 mm were placed symmetrically and uniformly in the internal space of each square steel tube (Fig. 1b). The bottom of each PVC hose was melted by fire and then squeezed together to seal. During the process of freezing, the air in the hollow PVC hoses was extruded out by the surrounding pressure resulted from the continuous expansion of the ice volume. In this way, the expansive pressure was released by the deformation of the PVC hoses, and the number of cracks in the ice core was greatly reduced. It should be admitted that the introduction of PVC hoses in ice could affect the mechanical properties of ice. However, it was assumed that this influence was small and compensated by the decrease of cracks in ice.

The bottoms of all PVC hoses in a specimen were connected to an iron wire ring, which held the PVC hoses to the bottom of the steel tube. Another ring, parallel to the bottom one, was attached to the top surface of the steel tube within the same plane to the hold the tops of the PVC hoses. When the eight PVC hoses were in place, adequate water was poured slowly into the steel tubes. It was carefully operated to avoid pouring water into the hollow space of PVC hoses. Otherwise, the function of PVC hoses would be lost. Then the square IFT specimens were placed in GDJS Temperature and Humidity Chamber to freeze for 48 h at −15 °C. After the specimens were taken from GDJS chamber, the top surface of them was ground to be smooth and flat using a grinding wheel with diamond cutters (Fig. 1d). It was found that the air in the hollow PVC hoses was totally squeezed out and the number of cracks in the ice core of square IFT specimens was greatly reduced. The preparation of square IFT specimens is illustrated in Fig. 1.

The manufacturing procedure of the circular plain ice specimens was almost identical to that of the square IFT columns. The square steel tube was replaced by a circular PVC tube with a height of 300 mm and an inner diameter of 150 mm. A 200 mm by 200 mm square waterproof board with a thickness of 10 mm was adhered to the bottom of the circular PVC tube as the bottom end-plate. Then the processes, including the placement of PVC hoses, water pouring, the freezing process in GDJS chamber and the grinding of specimens' upper surfaces, were identical to those of square IFT specimens. The PVC tube and the board were removed from each plain ice specimen prior to testing. Fig. 2 presents the preparation process of plain ice specimens.

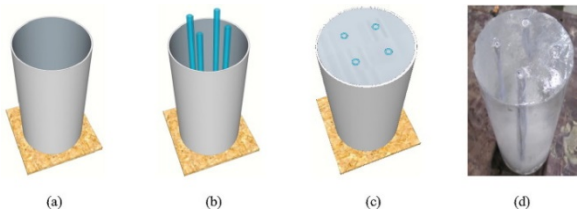

Fig. 2. Preparation of circular plain ice columns: (a) PVC formwork; (b) placement of PVC hoses; (c) ice specimen with formwork; and (d) ice specimen.

2.3. Material properties

Three tension coupons were cut from each type of steel tubes with thickness of 2 mm, 3 mm and 4 mm, respectively, to obtain the mechanical properties of the steel used in this study. All the tension coupons were made and tested in accordance with ASTM E8/E8M-15a [43]. Measured material properties of steel coupons with three different thicknesses, including the average values of elastic modulus E_s, yield strength f_y and tensile strength f_u, are reported in Table 1.

2.4. Instrumentation and testing

Layout of strain gauges for square IFT specimens is shown in Fig. 3. Two strain gauges perpendicular to each other in the longitudinal and transverse directions were glued at the mid-height of each side of the specimens to monitor the axial and hoop strains. Two pairs of strain gauges were installed away from the weld seams to avoid the complex stress state in these locations. The measured strains especially in the hoop directions might be influenced by this eccentric arrangement of strain gauges, but the eccentricity was so small that this influence was ignored. Glass cement was applied on the surface of each strain gauge for waterproof protection.

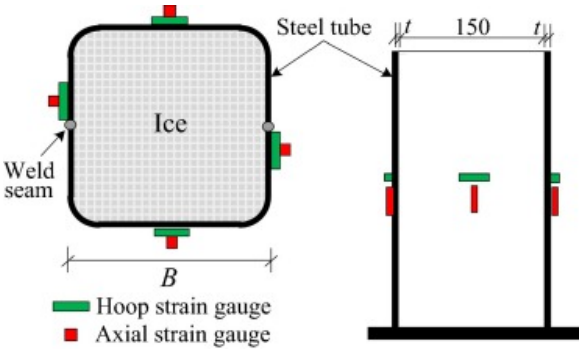

Fig. 3. Layout of strain gauges on square IFT specimens (Units in mm).

The experiments were conducted using a 3000 kN capacity compression machine under displacement control. Special attention was paid to the loading rate during the test. Artificial freshwater ice samples with a dimension of 7 cm × 7 cm × 17.5 cm were made and tested by Zhang et al [9] in 2011. The relationship between the uniaxial compressive strength and the strain rate at different temperatures was investigated. Three regions were observed corresponding to different strain rate. In the brittle region, the uniaxial compressive strength decreased with the increasing strain rate. In the ductile-brittle transition region, there was a change point of ductile-brittle, and the uniaxial compressive strength reached the maximum value. In the ductile region, the uniaxial compressive strength increased gradually with the increasing strain rate. The largest uniaxial compressive strength was reached under a strain rate between 10^{-4} s^{-1} and 10^{-2} s^{-1} at −5 °C. Based on their achievements, all specimens in this study were tested at a displacement control rate of 2 mm/min (i.e., strain rate of 1.11×10^{-4} s^{-1}). Two linear variable displacement transducers (LVDTs) were placed on opposite sides of each column to monitor the overall axial deformation. The schematic of the test setup is shown in Fig. 4. The

data of load, strains, and displacements of the specimen were recorded simultaneously by a data logger during the test.

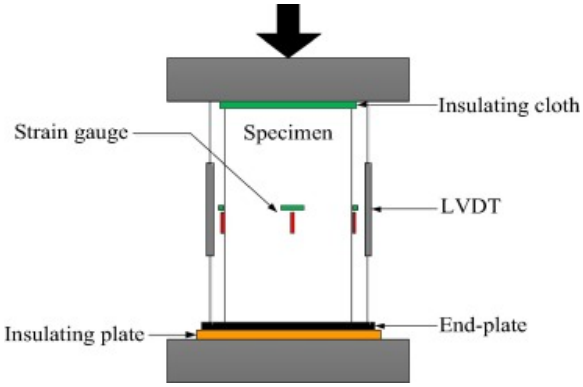

Fig. 4. Schematic of the test setup.

All the compression tests were conducted in January 2016 in Dalian, China, where the daily lowest temperature is normally below 0 °C in winter. Prior to and during the tests, all doors and windows of the laboratory were kept open. The tests were carried out when the temperature in the laboratory dropped to around −2 °C. An insulating plate was placed on the bottom of each plain ice or IFT specimen to achieve heat insulation between the specimen and the testing machine. The insulating plate was substituted by a piece of insulating cloth on the top of each IFT specimen because the upper insulating plate would get pierced by the steel tube of IFT columns without end-plate. For the plain ice columns, both ends of each specimen were wrapped by five layers of duct tape with a width of 5 cm to avoid premature damage in these regions.

3. Experimental results and discussion

3.1. Failure mode

The typical failure process of circular plain ice specimens subjected to uniaxial compression is shown in Fig. 5, which can be divided into three stages as following. First, minor cracks occurred randomly on the surface of the ice column. Second, the number of cracks increased with the increase of the load, and the cracks gradually developed towards the mid-height and inner of the specimens until the formation of major longitudinal cracks, which was accompanied by the sound of ice splitting. Third, plenty of cracks were observed and a big dilatation was found in the mid-height of each specimen in the ultimate stage. The ice was crushed due to lack of lateral confinement.

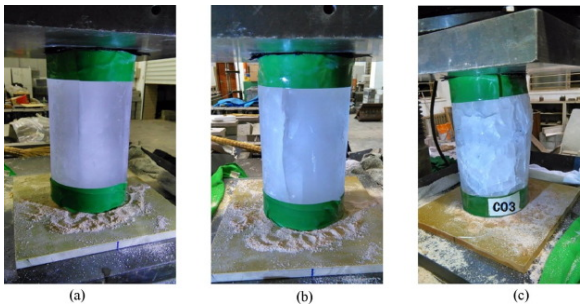

Fig. 5. Typical failure process of circular plain ice specimens: (a) slow development of cracks; (b) fast development of cracks; and (c) ultimate state of specimens.

The typical failure modes are shown in Fig. 6, Fig. 7 for hollow steel tubes and IFT columns, respectively. It can be seen in Fig. 6 that alternate inward and outward buckling deformations took place in the unfilled square steel

tubes, while all circular hollow steel tubes failed as outward local buckling occurring near the bottom end, termed elephant foot buckling [41]. For the IFT composite columns, the presence of the ice core prevented the occurrence of the inward buckling of the square steel tubes, resulting in only outward local buckling on the steel tubes' surfaces, as shown in Fig. 7. Outward local buckling was observed near the top end of all square IFT specimens, which was identical to that of the circular IFT columns due to lack of confinement from the steel end-plate at this location [41]. However, unlike circular composite columns, additional outward buckling was found at about 2/3 (Fig. 7d) or 1/3 height (Fig. 7h and 7i) of square IFT columns. In addition, the half-wavelengths produced by local buckling for the square IFT sections were considerably smaller than those for the hollow square steel tubes without the help of ice. This phenomenon was also found in square CFT columns [33]. The reduced wavelength was a major factor for the increase in load bearing capacity at which local buckling occurs. It was an interesting phenomenon that some of the cracks observed in the top surface of the ice core achieved self-healing after the compression test at −2 °C. This feature would have a positive effect on the long-term performance of the IFT columns. Unfortunately, the failure mode of the ice core could not be checked by removing the outer steel tubes with flame cutting because the ice would be disturbed or even destroyed during this process.

(a) H21 (b) H31 (c) H41

Fig. 6. Typical buckling modes observed for hollow steel tubes.

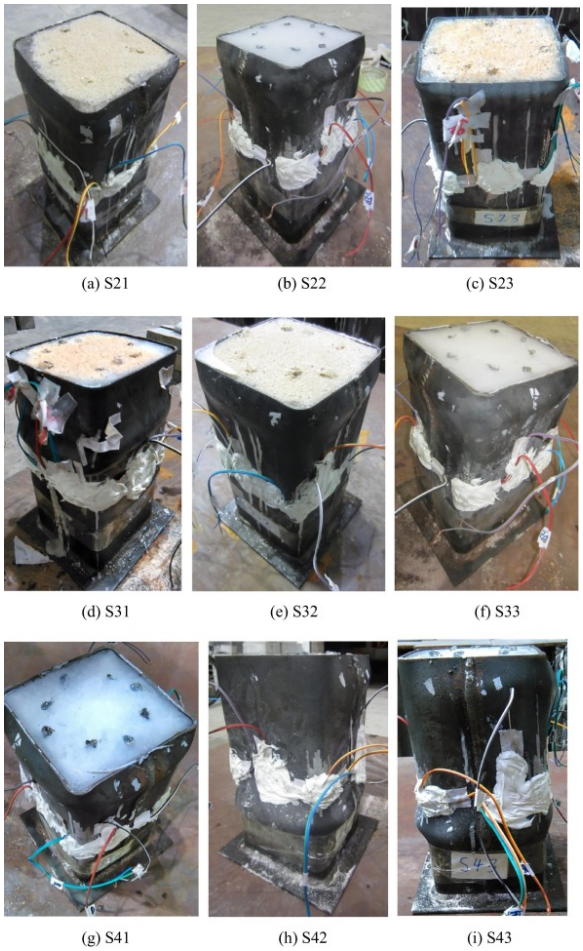

Fig. 7. Failure modes observed for square IFT specimens.

3.2. Load vs. deformation response

The axial load vs. shortening curves of circular plain ice specimens under axial compression are shown in Fig. 8. The load increased linearly with the axial deformation before reaching approximately 70% of the peak load. Then the ice specimens entered plastic state and a descending branch occurred after the peak load. It is interesting that the descending branch of the axial load vs. shortening curve for ice is not very steep compared with that of concrete. Therefore, the ice exhibited some level of ductile behavior under the conditions with test temperature of −2 °C and loading rate of 2 mm/min in this study. The compressive strength of unconfined ice was 3.45 MPa calculated by averaging the strength values of the three plain ice specimens.

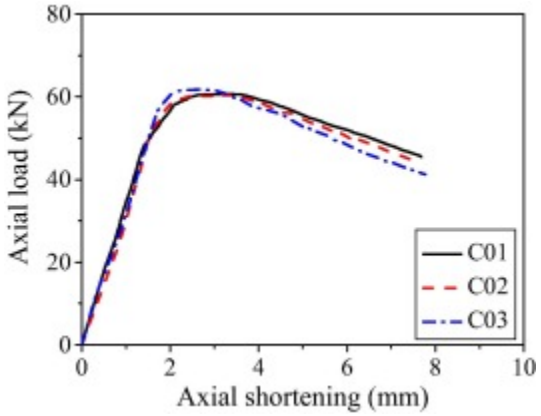

Fig. 8. Axial load vs. shortening curves of plain ice specimens.

In order to better compare the responses of identical steel sections with and without ice core, the axial load vs. shortening results of each series for the hollow square steel tubes and the IFT specimens are presented in Fig. 9. It was observed that the initial stiffness of the square IFT specimens was almost the same as that of the hollow steel tubes with the same dimensions because the elastic modulus of the steel (around 200 GPa) is much larger than that of the ice (around 0.5 GPa obtained from Fig. 8), which was also found in the compression test of the circular IFT columns [41]. By contrast, the initial stiffness of the traditional CFT columns is much larger than that of the steel tubes without inner concrete [32]. Within the same series of specimens, the peak load of an ice-filled section was obviously higher than that observed for the corresponding steel tube. The average load bearing capacity of IFT specimens with 2 mm thick steel tubes was 24.6% higher than the one measured from the hollow steel tubes within the same series. For specimens in series c and d, the enhancements were 21.3% and 22.4%, respectively.

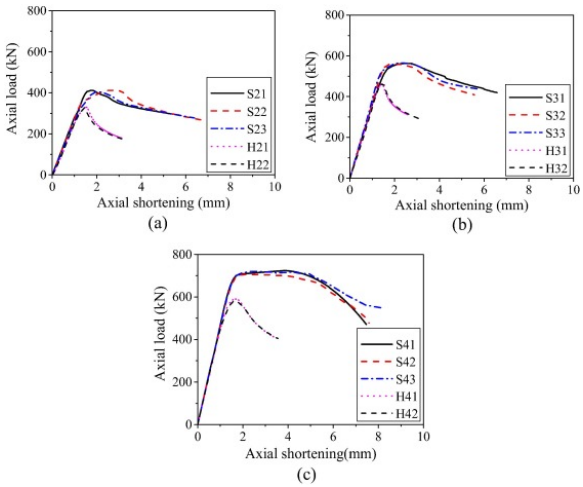

Fig. 9. Axial load vs. shortening curves of hollow square steel tubes and IFT specimens under axial compression: (a) 2-mm-thick tube; (b) 3-mm-thick tube; and (c) 4-mm-thick tube.

Three typical square IFT specimens (i.e., S23, S33 and S41) were selected to investigate the influence of width-to-thickness (B/t) ratio of the steel tubes on the axial load vs. deformation curves, as shown in Fig. 10. The initial stiffness and peak load increased with the decrease of B/t ratio. The IFT specimen with a smaller B/t ratio had higher strength and better ductility. There was even a platform branch observed for the axial load vs. deformation curve of specimen S41 (B/t = 39.5), where the axial load remained about 700 kN while the axial deformation increased from 2 mm to 4 mm.

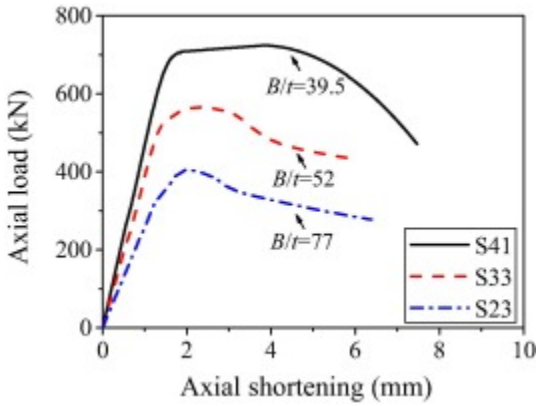

Fig. 10. The influence of B/t ratio on axial load vs. deformation curves of IFT specimens.

Axial load vs. deformation curves of plain ice specimens, hollow steel tubes, IFT specimens, and the superposition of the first two are plotted in Fig. 11. In fact, the axial load vs. deformation responses of the hollow steel tubes with the same thickness are very close to each other (Fig. 9). Therefore, the experimental results of H22, H32 and H41 were selected as representatives for those of hollow steel tubes with a thickness of 2 mm, 3 mm and 4 mm, respectively. Similarly, the test result of C02 was chosen as a representative constitutive curve for plain ice. By keeping the stress identical between square and circular plain ice columns, the load values of C02 were changed proportionally to the areas between square and circular columns to obtain the axial load vs. deformation curve of a square plain ice column shown in Fig. 11. The superposition results of plain ice columns and hollow steel tubes were obtained by simple summation of the axial load of ice and steel corresponding to the same deformations. The peak load carried by steel tube was much larger than that carried by ice. The initial stiffness of steel tubes, IFT columns, and the superposition of ice and steel was very close to each other. The peak loads of the square IFT columns with tube thickness of 2 mm, 3 mm and 4 mm were 1.06, 1.07 and 1.10 times, respectively, as large as the summations of the strengths of the inner ice and steel tubes. It confirmed that there existed more remarkable composite actions between the inner ice and the outer square steel tubes with a smaller B/t ratio. However, a slightly downward trend of the composite action was observed in the circular IFT columns with the increasing tube thickness [41]. The bearing capacities of circular IFT columns were 1.10, 1.06 and 1.04 times as large as the superposition results of the two parts alone [41]. It is believed that the difference in the composite action between square and circular IFT columns is related to the cross-sectional properties as well as the material properties. It should be noted that there was not steel end-plate welded to the top of IFT specimens to avoid disturbing or even destroying the ice in the process of welding. However, the hollow steel tubes had end-plates welded to both ends, which should help hollow steel tubes to obtain a better behavior than that of hollow tubes with one end-plate. Therefore, the difference between the capacities of IFT specimens and superposition results of plain ice and steel hollow tubes would be larger if the hollow tubes were welded only one end-plate. The square IFT specimens tested in this study exhibited higher bearing capacity and better ductility than those of the summation of ice and steel tube, which can be explained by the following two reasons. Firstly, the bucking modes of the outer steel tubes in IFT specimens were greatly influenced by the ice core and the inward local buckling was delayed or suppressed. Secondly, the ice core was in triaxial compression stress state due to the confinement from the outer steel tube, leading to a great increase in strength.

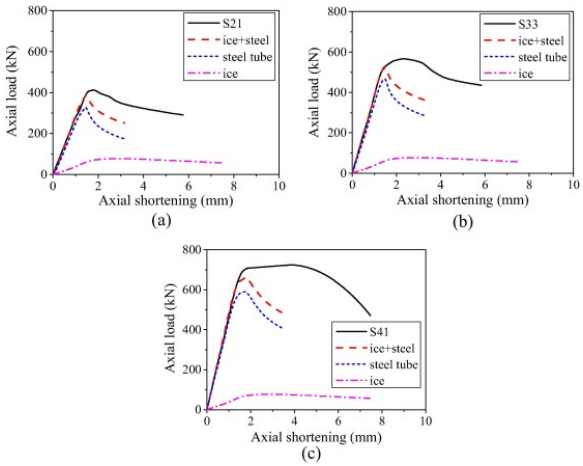

Fig. 11. Comparisons of axial load vs. shortening curves between plain ice columns, steel tubes, IFT columns, and the summation of ice and steel.

3.3. Load vs. strain behavior of IFT columns

The axial load vs. strain curves of the square IFT specimens are shown in Fig. 12. Both the hoop and axial strains were obtained by averaging the readings of the strain gauges installed at the mid-height of the IFT specimens. In the initial stage (i.e., elastic branch), both the axial and hoop strains increased approximately in a linear manner with the increase of the load, and the growth rates of axial strains were obviously faster than those of hoop strains. The confinement effect was very small at this stage because the Poisson's ratio of ice (around 0.3 [11], [44]) is close to that of steel (around 0.3 for low-carbon steel [45]). There was almost no interaction between ice and steel tubes in this stage, and therefore the ice was under uniaxial compression stress state. As the load increased, the lateral expansion of the ice gradually became greater than that of the outer steel tube due to cracking of the ice which accelerated the deformation of ice in hoop direction, and therefore a radial pressure developed at the ice-steel interface. The confinement to the ice core was achieved and the ice core was in triaxial compression stress state. The outer steel tube was subjected to axial compressive and hoop tensile stresses. In this stage (i.e., plastic branch), the axial load vs. strain curves featured a gentle ascending branch and the measured hoop strains started to increase quickly as shown in Fig. 12, which was roughly corresponding to the peak load stage of the plain ice. In the last stage (i.e., descending branch), the inner ice was crushed and the composite action between ice and steel tube was reduced, which caused the slower increase in hoop strains while the axial strains continued to increase until failure. On the whole, the axial load vs. strain responses of the square IFT columns were similar to those of the circular IFT columns [41], which can be divided into three stages corresponding to elastic branch, plastic branch and descending branch, respectively. The key difference between the square and circular IFT columns [41] was observed in the plastic branch. The axial load increased slowly with the increasing axial strain for the square IFT columns. By contrast, the axial load of the circular IFT columns remained almost constant with the increasing axial strain.

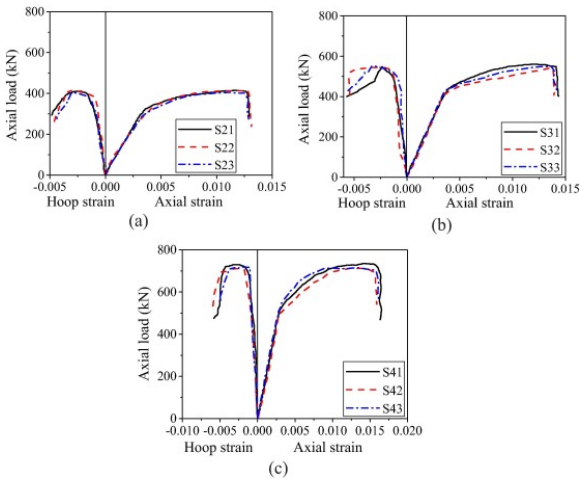

Fig. 12. Axial load vs. strain curves of IFT specimens: (a) 2-mm-thick tube; (b) 3-mm-thick tube; and (c) 4-mm thick tube.

4. Axial bearing capacity of IFT stub columns

One calculation method is proposed in this study to predict the axial bearing capacity of square IFT stub columns. In the composite column, the force along the thickness direction of the wall of the hollow tube is so small that it can be neglected because the wall is thin. Therefore, the steel can be considered under the state of plane-stress [45]. The occurrence of hoop tension in steel results in the decrease of the maximum value of the axial compressive stress. Two major assumptions are made in this theoretical study for simplification. One is that the stresses in the cross-sections of both steel and ice are uniformly distributed. The other is that the steel tube yields when the IFT specimen reaches its peak load. The axial bearing capacity of square IFT stub columns N_u can be predicted by

(1) $N_u = f_v A_s + f_{ci} A_i$

where A_i and A_s are the cross-sectional areas of ice and steel section, respectively; f_v is the axial compressive stress of the steel tube corresponding to the peak load; f_{ci} is the compressive strength of confined ice and its calculation is based on the equation proposed by Mander et al. [46] for confined concrete:

(2) $f_{ci} = f_i \left(-1.254 + 2.254 \sqrt{1 + 7.94 \frac{f_r}{f_i}} - 2 \frac{f_r}{f_i} \right)$

where f_i is the compressive strength of unconfined ice and its value is 3.45 MPa obtained from the average test results of three plain ice specimens in this study; f_r is the confining stress of the square steel tube on the ice and it can be calculated as following based on static equilibrium:

(3) $f_r = \frac{2 f_h t}{D - 2t}$

where f_h is the hoop stress of the steel tube corresponding to the peak load.

It is assumed that the steel yields when the IFT specimen reaches the peak load. The yield of steel tube follows the Von Mises criterion in the following form:

(4) $f_v^2 + f_h^2 - f_v f_h = f_y^2$

Based on Eq. (4), the hoop stress of the steel tube can be calculated by

(5) $f_h = -\frac{f_v}{2} + \sqrt{f_y^2 - \frac{3}{4} f_v^2}$

The analysis method proposed by Zhang et al. [47] was adopted to obtain the compressive strength of the steel tube when the IFT specimen reached its ultimate bearing capacity, which is given as

(6) $\frac{f_v}{f_y} = \alpha + \beta ln \xi$

(7) $\xi = \frac{f_y A_s}{f_i A_i}$

where α and β are two coefficients obtained after trials and analysis. ξ is the confinement ratio initially proposed for CFT columns and hereon it is used for the IFT specimens. It should be noted that the value of ξ for the IFT specimens is general larger than 1.0 while its value is smaller than 1.0 in concrete filled steel tube because the ice is so weak compared with concrete.

If the values of α and β were given, the axial bearing capacity of square IFT columns could be obtained by using Eqs. (1), (2), (3), (4), (5), (6), (7). To find the best values of α and β, an evaluation coefficient r was introduced and given by

(8) $r = \sqrt{\sum_{n=1}^{9} \left(\frac{N_{e(n)} - N_{u(n)}}{N_{e(n)}} \right)^2}$

where $Nu(n)$ and $Ne(n)$ are the bearing capacities of the nth IFT specimen obtained from calculation and experiment, respectively. The values of n ranged from one to nine because there are nine square IFT specimens tested in this study. A smaller value of r indicated that the calculated results are closer to the experimental ones. After plenty of trials and analysis, the coefficient r reached its minimum value when the values of α and β were taken as −1.17 and 0.90, respectively.

The comparison between experimental and calculated results is reported in Table 1 and Fig. 13. The values of calculated axial load strength N_u using Eq. (1) are very close to those of the axial load strength N_e obtained from experimental results. Therefore, the values of N_u/N_e are close to 1, which indicates that the proposed axial bearing capacity equation for square IFT stub columns can provide accurate predictions of the test results. The relative errors are within ±2%. The applicable range for the proposed method to calculate the axial load strength of square IFT stub columns is $39.5 \le B/t \le 77$. It should be admitted that the number of IFT specimens tested in this study is very small, and more parameters such as the temperature and loading rate need to be investigated. In addition of ice, the mechanical properties of steel are also influenced by the Arctic low temperature. The results of tensile tests conducted at −80 °C, −60 °C, −40 °C, −20 °C, 0 °C, and 30 °C revealed that the mechanical properties of steel including yield strength, ultimate strength, and elastic modulus increased as the temperature decreased [48], [49]. Therefore, the composite interaction and strength of the square IFT columns might be affected by additional variables such as temperature, and it is worth to take more test variable into consideration. However, it is beyond the scope of the current study (developing and validating square IFT as a new construction component). This will be studied in future by the authors or other interested researchers. The proposed equation will also be further refined by experimental and analytical results of more specimens with more parameters in further research.

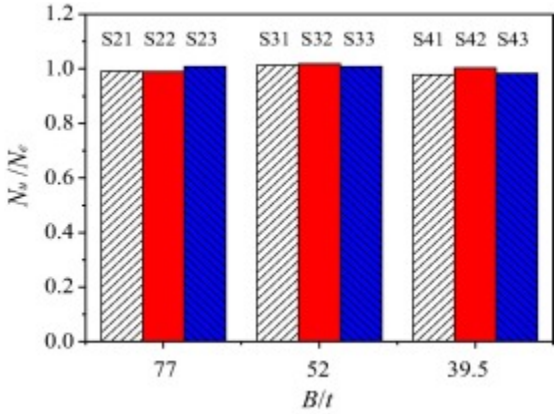

Fig. 13. Comparisons between experimental and calculated results.

5. Conclusions

The innovative square ice filled steel tube (IFT) column was proposed in this study, which effectively combined the advantages of ice and steel tubes. When the square IFT column is subjected to axial compression, the load is carried by both the ice core and the outer steel tube simultaneously. The enhancement of structural properties of square IFT columns is mainly due to the composite action of steel hollow section and ice core. The confining effect from the steel hollow section causes the ice core to behave in a triaxial stress state while the ice core prevents the wall of the steel hollow section from buckling inward. Therefore, there is a great improvement in the bearing capacity and the ductility of IFT columns. Other advantages of IFT columns include: (a) More economical construction in the cold regions: plain ice is easily acquired in these regions and only shipping hollow steel tubes is much cheaper than shipping steel and components of concrete to these regions; (b) Greater ease for construction: the construction process is easy and fast due to the elimination of formwork. Therefore, the proposed IFT columns have potential to be widely used in the building constructions in cold regions.

In this study, the axial compressive behavior of the proposed IFT stub columns was experimentally investigated. The influence of width-to-thickness (B/t) ratio of steel tube on the behavior of square IFT stub columns was analyzed. Based on the present experimental and theoretical investigation, the following conclusions can be drawn:

1. The IFT columns exhibited higher strength and better ductility than those of the summation of hollow steel tubes and plain ice columns, which confirms the remarkable composite action between the ice core and the outer steel tube.
2. The initial stiffness of IFT columns was similar to that of hollow steel tubes.
3. The initial stiffness and ultimate bearing capacity of the IFT stub columns increased with the decrease of B/t ratio (varying from 39.5 to 77).
4. A simplified equation for predicting the axial bearing capacity of IFT stub columns was proposed and it agreed well with the experimental results.

Conflict of interest

None.

Acknowledgments

This work was supported by the National Key R&D Program of China, China (Grant No. 2017YFC0703008), the National Natural Science Foundation of China (Project No. 51778102), the Fundamental Research Funds for the Central Universities (Project No. DUT18LK35) and the State Scholarship Fund of China (Project No. 201706060249).

References

[1] R.L. Handy **Igloo and natural bridge as ultimate structures** *Arctic*, 26 (1976), pp. 276-281

[2] E.M. Schulson **The brittle compressive fracture of ice** *Acta Metall. Mater*., 38 (1990), pp. 1963-1976

[3] E.M. Schulson, S.E. Buck **The ductile-to-brittle transition and ductile failure envelopes of orthotropic ice under biaxial compression** *Acta Metall. Mater*., 43 (1995), pp. 3661-3668

[4] J. Weiss, E.M. Schulson **The failure of fresh-water granular ice under multiaxial compressive loading** *Acta Metall. Mater*., 43 (1995), pp. 2303-2315

[5] J. Xiao, I.J. Jordaan **Application of damage mechanics to ice failure in compression** *Cold Reg. Sci. Technol*., 24 (1996), pp. 305-322

[6] M. Arakawa, N. Maeno **Mechanical strength of polycrystalline ice under uniaxial compression** *Cold Reg. Sci. Technol*., 26 (1997), pp. 215-229

[7] S.J. Jones **High strain-rate compression tests on ice** *J. Phys. Chem. B*, 101 (1997), pp. 6099-6101

[8] E.M. Schulson, E.T. Gratz **The brittle compressive failure of orthotropic ice under triaxial loading** *Acta Mater*., 47 (1999), pp. 745-755

[9] L.M. Zhang, Z.J. Li, Q. Jia, G.W. Li, W.F. Huang**U niaxial compressive strengths of artificial freshwater ice** *Adv. Mater. Res*., 243–249 (2011), pp. 4634-4637

[10] D.M. Masterson **State of the art of ice bearing capacity and ice construction** *Cold Reg. Sci. Technol*., 58 (2009), pp. 99-112

[11] J.J. Petrovic **Mechanical properties of ice and snow** *J. Mater. Sci*., 38 (2003), pp. 1-6

[12] P.D. Barrette, I.J. Jordaan **Pressure-temperature effects on the compressive behavior of laboratory-grown and iceberg ice** *Cold Reg. Sci. Technol*., 36 (2003), pp. 25-36

[13] S.J. Jones, H.A.M. Chew **Creep of ice as a function of hydrostatic pressure** *J. Phys. Chem*., 87 (1983), pp. 4064-4066

[14] P. Kalifa, G. Ouillon, P. Duval **Microcracking and the failure of polycrystalline ice under triaxial compression** *J. Glaciol*., 38 (1992), pp. 65-76

[15] Y.L. Wang, Y.S. Wang, B. Wan, B.G. Han, G.C. Cai, Z.Z. Li **Properties and mechanisms of self-sensing carbon nanofibers/epoxy composites for structural health monitoring** *Compos. Struct*., 200 (2018), pp. 669-678

[16] Y. Mizuno **Effect of hydrostatic confining pressure on the failure mode and compressive strength of polycrystalline ice** *J. Phys. Chem. B*, 102 (1998), pp. 376-381
[17] P.K. Dutta, D.M. Cole, E.M. Schulson, D.S. Sodhi **A fracture study of ice under high strain rate loading** *Int. J. Offshore Polar Eng.*, 14 (2004), pp. 182-188
[18] P.O. Moslet **Field testing of uniaxial compression strength of columnar sea ice** *Cold Reg. Sci. Technol.*, 48 (2007), pp. 1-14
[19] M. Shazly, V. Prakash, B.A. Lerch **High strain-rate behavior of ice under uniaxial compression** *Int. J. Solids Struct.*, 46 (2009), pp. 1499-1515
[20] L.M. Zhang, Z.J. Li, Q. Jia, W.F. Huang **Experimental study on uniaxial compressive strength of reservoir ice** *Trans. Tianjin Univ.*, 18 (2012), pp. 112-116
[21] M.F. Perutz **A description of the iceberg aircraft carrier and the bearing of the mechanical properties of frozen wood pulp upon some problems of glacier flow** *J. Glaciol.*, 1 (1948), pp. 95-104
[22] W.A. Nixon, R.A. Smith **The fracture toughness of some wood-ice composites** *Cold Reg. Sci. Technol.*, 14 (1987), pp. 139-145
[23] W.A. Nixon **Alluvium-reinforced ice: a preliminary report of bending strength tests** *Cold Reg. Sci. Technol.*, 16 (1989), pp. 309-313
[24] N.K. Vasiliev **On development of fibre-ice-composites** *Cold Reg. Sci. Technol.*, 21 (1993), pp. 195-199
[25] N.K. Vasiliev, A.A. Ivanov, I.N. Shatalina, V.V. Sokurov **Ice- and cryogel-soil composites in water-retaining elements in embankment dams constructed in cold regions** *Sci. Cold Arid Reg.*, 5 (2013), pp. 444-450
[26] N.K. Vasiliev, A.A. Ivanov, V.V. Sokurov, I.N. Shatalina, K.N. Vasilyev **Strength properties of ice-soil composites created by method of cryotropic gel formation** *Cold Reg. Sci. Technol.*, 70 (2012), pp. 94-97
[27] V.I. Lozinsky **A brief history of polymeric cryogels** O. Okay (Ed.), *Polymeric Cryogels*, Springer International Publishing, New York (2014), pp. 1-48
[28] N.K. Vasiliev, A.D.C. Pronk, I.N. Shatalina, F.H.M.E. Janssen, R.W.G. Houben **A review on the development of reinforced ice for use as a building material in cold regions** *Cold Reg. Sci. Technol.*, 115 (2015), pp. 56-63
[29] Z.B. Wang, Z. Tao, L.H. Han, B. Uy, D. Lam, W.H. Kang **Strength, stiffness and ductility of concrete-filled steel columns under axial compression** *Eng. Struct.*, 135 (2017), pp. 209-221
[30] H. Ge, T. Usami **Strength of concrete-filled thin-walled steel box columns: experiment** *J. Struct. Eng.*, 118 (1992), pp. 3036-3054
[31] D.L. Liu, W.M. Gho, J. Yuan **Ultimate capacity of high-strength rectangular concrete-filled steel hollow section stub columns** *J. Constr. Steel Res.*, 59 (2003), pp. 1499-1515
[32] L.H. Han, W. Li, R. Bjorhovde **Developments and advanced applications of concrete-filled steel tubular (CFST) structures: members** *J. Constr. Steel Res.*, 100 (2014), pp. 211-228
[33] L.H. Guo, S.M. Zhang, W.J. Kim, G. Ranzi **Behavior of square hollow steel tubes and steel tubes filled with concrete** *Thin-Walled Struct.*, 45 (2007), pp. 961-973
[34] M.V. Chitawadagi, M.C. Narasimhan, S.M. Kulkarni **Axial capacity of rectangular concrete-filled steel tube columns – DOE approach** *Constr. Build. Mater.*, 24 (2010), pp. 585-595
[35] Y.S. Du, Z.H. Chen, M.X. Xiong **Experimental behavior and design method of rectangular concrete-filled tubular columns using Q460 high-strength steel** *Constr. Build. Mater.*, 125 (2016), pp. 856-872
[36] C.H. Lee, T.H.K. Kang, S.Y. Kim, K. Kang **Strain compatibility method for the design of short rectangular concrete-filled tube columns under eccentric axial loads** *Constr. Build. Mater.*, 121 (2016), pp. 143-153
[37] L.H. Han **Flexural behaviour of concrete-filled steel tubes** *J. Constr. Steel Res.*, 60 (2004), pp. 313-337
[38] M.X. Xiong, D.X. Xiong, J.Y.R. Liew **Flexural performance of concrete filled tubes with high tensile steel and ultra-high strength concrete** *J. Constr. Steel Res.*, 132 (2017), pp. 191-202
[39] G.C. Li, D. Liu, Z.J. Yang, C.Y. Zhang **Flexural behavior of high strength concrete filled high strength square steel tube** *J. Constr. Steel Res.*, 128 (2017), pp. 732-744

[40] M. Yu, X.Y. Pei, L.H. Xu, J.Q. Ye **A unified formula for calculating bending capacity of solid and hollow concrete-filled steel tubes under normal and elevated temperature** *J. Constr. Steel Res*., 141 (2018), pp. 216-225

[41] Y.L. Wang, G.P. Chen, B. Wan, H. Lin, J. Zhang **Behavior of innovative circular ice filled steel tubular stub columns under axial compression** *Constr. Build. Mater*., 171 (2018), pp. 680-689

[42] J. Schwarz, R. Frederking, V. Gavrillo, I.G. Petrov, K.I. Hirayama, M. Mellor, P. Tryde, K.D. Vaudrey **Standardized testing methods for measuring mechanical properties of ice** *Cold Reg. Sci. Technol*., 4 (1981), pp. 245-253

[43] ASTM E8/E8M-15a, Standard Test Methods for Tension Testing of Metallic Materials, West 2015 Conshohocken, PA.

[44] L.W. Gold **Some observations on the dependence of strain on stress for ice** *Can. J. Phys*., 36 (1958), pp. 1265-1275

[45] S.T. Zhong **Concrete-Filled Steel Tubular Structures** (Third ed.), Tsinghua University Press, Beijing (2003) (in Chinese)

[46] J.B. Mander, M.J.N. Priestley, R. Park **Theoretical stress-strain model for confined concrete** *J. Struct. Eng*., 114 (1988), pp. 1804-1826

[47] S.M. Zhang, L.H. Guo, Z.L. Ye, Y.Y. Wang **Behavior of steel tube and confined high strength concrete for concrete-filled RHS tubes** *Adv. Struct. Eng*., 8 (2005), pp. 101-116

[48] J.B. Yan, J.Y.R. Liew, M.H. Zhang, J.Y. Wang **Mechanical properties of normal strength mild steel and high strength steel S690 in low temperature relevant to Arctic environment** *Mater. Des*., 61 (2014), pp. 150-159

[49] J.B. Yan, X.M. Liu, J.Y.R. Liew, X.D. Qian, M.H. Zhang **Steel-concrete-steel sandwich system in Arctic offshore structure: materials, experiments, and design** *Mater. Des*., 91 (2016), pp. 111-121